



Research paper

Microtubule associated protein 4 phosphorylation leads to pathological cardiac remodeling in mice



Lingfei Li ^{a,b}, Qiong Zhang ^{a,b}, Xingyue Zhang ^{a,b}, Junhui Zhang ^{a,b}, Xuefeng Wang ^c, Jun Ren ^d, Jiezhai Jia ^{a,b}, Dongxia Zhang ^{a,b}, Xupin Jiang ^{a,b}, Jiaping Zhang ^{b,e}, Hao Mei ^f, Bing Chen ^g, Jiongyu Hu ^{b,g,**}, Yuesheng Huang ^{a,b,*}

^a Institute of Burn Research, Southwest Hospital, Third Military Medical University (Army Medical University), Chongqing, China

^b State Key Laboratory of Trauma, Burns and Combined Injury, Southwest Hospital, Third Military Medical University (Army Medical University), Chongqing, China

^c Department of Cardiovascular Surgery, Xinqiao Hospital, Third Military Medical University (Army Medical University), Chongqing, China

^d Center for Cardiovascular Research and Alternative Medicine, University of Wyoming College of Health Sciences, Laramie, WY, USA

^e Department of Plastic Surgery, Southwest Hospital, Third Military Medical University (Army Medical University), Chongqing, China

^f Center for Outcomes Research and Evaluation, Yale-New Haven Hospital, CT, USA

^g Endocrinology Department, Southwest Hospital, Third Military Medical University (Army Medical University), Chongqing, China

ARTICLE INFO

Article history:

Received 8 August 2018

Received in revised form 23 September 2018

Accepted 8 October 2018

Available online 13 October 2018

Keywords:

MAP4

Cardiac remodeling

Apoptosis

Mitochondria

Microtubule

ABSTRACT

Background: Cardiac remodeling is a pathophysiological process that involves various changes in heart, including cardiac hypertrophy and fibrosis. Cardiac remodeling following pathological stimuli is common trigger leading to cardiac maladaptation and onset of heart failure, and their pathogenesis remains unclear.

Methods: Heart specimens of tetralogy of Fallot (TOF) patients, myocardial infarction (MI) and transverse aortic constriction (TAC) mouse models were collected to determine changes of microtubule associated protein 4 (MAP4) phosphorylation. MAP4 (S667A, S737E and S760E) knock in (MAP4 KI) mouse and cultured neonatal mouse cardiomyocytes or fibroblasts were used to investigate changes of cardiac phenotypes and possible mechanisms with a variety of approaches, including functional, histocytological and pathological observations.

Findings: Elevated cardiac phosphorylation of MAP4 (S737 and S760) was observed in TOF patients, MI and TAC mouse models. In MAP4 KI mice, age-dependent cardiac phenotypes, including cardiac hypertrophy, fibrosis, diastolic and systolic dysfunction were observed. In addition, increased cardiomyocyte apoptosis together with microtubule disassembly and mitochondrial translocation of phosphorylated MAP4 was detected prior to the onset of cardiac remodeling, and p38/MAPK was demonstrated to be the possible signaling pathway that mediated MAP4 (S737 and S760) phosphorylation.

Interpretation: Our data reveal for the first time that MAP4 drives pathological cardiac remodeling through its phosphorylation. These findings bear the therapeutic potential to ameliorate pathological cardiac remodeling by attenuating MAP4 phosphorylation.

Fund: This work was supported by the Key Program of National Natural Science Foundation of China (No.81430042) and National Natural Science Foundation of China (No.81671913).

© 2018 The Authors. Published by Elsevier B.V. This is an open access article under the CC BY-NC-ND license (<http://creativecommons.org/licenses/by-nc-nd/4.0/>).

1. Introduction

Cardiac remodeling is a cellular response to a variety of stimuli, characterized by cardiac hypertrophy and fibrosis. Pathological cardiac remodeling is a major risk factor for the development of chronic heart failure, an ultimate sequelae for a variety of heart diseases responsible for high mortality (~50% for 5 years) [1,2]. Cardiac remodeling is often attributed to the presence of sustained pathological stimuli including hypoxia, myocardial infarction (MI), pressure or volume overload [3,4]. Although the hypertrophic and fibrotic response provides early adaptive compensation, these remodeling events are deemed

* Correspondence to: Y. Huang, Institute of Burn Research, State Key Laboratory of Trauma, Burns and Combined Injury, Southwest Hospital, Third Military Medical University (Army Medical University), Gaotanyan Street, Shapingba District, Chongqing 400038, China.

** Correspondence to: J. Hu, Endocrinology Department, State Key Laboratory of Trauma, Burns and Combined Injury, Southwest Hospital, Third Military Medical University (Army Medical University), Gaotanyan Street, Shapingba District, Chongqing 400038, China.

E-mail addresses: jiongyuhu@163.com (J. Hu), yshuang1958@163.com (Y. Huang).

Research in context

Evidence before this study

Apoptosis and cytoskeleton played an important role in regulating cardiac remodeling, and the detailed mechanism was elusive. Microtubule associated protein 4 (MAP4) was found an important factor in regulating cardiomyocyte apoptosis and microtubule dynamics, however, whether MAP4 was involved in cardiac remodeling was still unknown.

Added value of this study

Increased cardiac phosphorylation of MAP4 (S737 and S760) was detected in tetralogy of Fallot patients, myocardial infarction and transverse aortic constriction mouse models. And age-dependent cardiac remodeling was observed in MAP4 (S667A, S737E and S760E) knock in (MAP4 KI) mouse. In addition, increased cardiomyocyte apoptosis together with microtubule disassembly and mitochondrial translocation of phosphorylated MAP4 was detected prior to the onset of cardiac remodeling, and p38/MAPK was found to be the possible signaling pathway that mediated MAP4 (S737 and S760) phosphorylation.

Implications of all the available evidence

Our findings reveal that MAP4 phosphorylation may serve as a springboard for the pathogenesis of multiple cardiomyopathies including cardiac hypertrophy, fibrosis, diastolic and systolic dysfunction, suggesting its therapeutic potentials in these comorbidities.

maladaptive and may predispose to the ever-rising cardiovascular morbidity and mortality along with loss of cardiomyocytes through cell death machineries such as necrosis, apoptosis, or possibly excessive autophagy [5–8]. However, the precise mechanisms through which cardiomyocytes sense and respond to the force patterns imposed by overload or hypoxia/ischemia, and how cardiomyocyte death pathways are activated, remains elusive. Therefore, a comprehensive understanding of biological processes leading to heart disease in particularly pathological cardiac remodeling is required.

Cytoskeleton rearrangement is regarded to play an important role in the cardiac remodeling. Microtubule-associated proteins (MAPs) are well known as cytosolic skeleton proteins bound to tubulin to stimulate their polymerization. The assembly-promoting MAPs include MAP2, tau and MAP4. MAP4 is ubiquitously expressed in non-neural cells and possesses an important role in microtubule (MT) dynamics [9–12]. In addition, MAP-MT binding is regulated through MAPs phosphorylation, which leads to the detachment of MAPs from MT and subsequent destabilization of the MT [13,14]. We and others have reported that the sites S696, S768 and S787 in the proline-rich region of MT-binding domain of human MAP4 are critical sites for phosphorylation governing its detachment from MTs [10,15,16], and that mitogen-activated protein kinase 6 (MKK6)/p38 MAPK is the upstream signaling for hypoxia-induced MAP4 phosphorylation with subsequent MT disassembly [17]. There is also *in vitro* evidence for a crucial role for phosphorylated MAP4 (p-MAP4) in the pathophysiological process of cardiac mitochondrial dysfunction and apoptosis. p-MAP4 detached from MTs is found to be translocated to mitochondria from cytosol, leading to mitochondrial permeability transition pore opening and apoptosis [13]. However, the clinical and *in vivo* implication of MAP4 phosphorylation is still debatable as that seen in cardiomyocytes.

Here in this study, we examined, for the first time, levels of p-MAP4 in the hypertrophic right ventricular tissues in patients with tetralogy of Fallot (TOF). TOF patients are characterized by low arterial oxygen saturation (SaO₂) and right ventricular hypertrophy. In order to clarify the effect of hypoxia and hypertrophy (induced by pressure overload) on MAP4 phosphorylation separately, MI and transverse aortic constriction (TAC) mouse models, denoting hypoxia- and pressure overload-related diseases, respectively, were applied. Subsequently, to investigate the effect of aberrant MAP4 phosphorylation *in vivo*, we generated mice that mimicked MAP4 hyperphosphorylation at specific sites (S737 and S760) based on the findings in TOF patients and TAC mouse models. To our surprise, MAP4 hyperphosphorylation triggered cardiac remodeling with aging, accompanied with increased cardiomyocyte apoptosis. MT disassembly and mitochondrial translocation of p-MAP4 in cardiomyocytes were deemed the possible mechanisms of apoptosis, contributing to the process of cardiac remodeling. Collectively, these findings gave a novel insight for MAP4 phosphorylation (S737 and S760) in promoting cardiac apoptosis and remodeling, indicating its therapeutic potential in the prevention and treatment of cardiac remodeling and related diseases.

2. Materials and methods

2.1. Myocardium biopsy specimen collection in TOF patients

Fresh right ventricular tissues were collected from 16 TOF patients with hypoxemia (SaO₂ < 90%; n = 8) or normal blood oxygen (SaO₂ ≥ 90%; n = 8) in the Department of Cardiovascular Surgery, Xinqiao Hospital, Chongqing, China. Myocardial specimens were collected from patients with TOF undergoing surgery, mainly from hypertrophic right ventricular myocardium, and were divided into two groups depending on the levels of SaO₂ upon admission (Tables S1 and S2). TOF diagnosis was based on the American Heart Association criteria. Equivalence of two means power analysis was used to estimate sample size. The investigator was blinded to the group allocation in the experimental procedure and when assessing the outcome. Preoperative characteristics of these patients were summarized in Table S1. Intraoperative anesthetic and operative techniques were standardized, and ventricular biopsy specimens (100 mg net weight) were collected from right ventricles and were stored immediately. The pathological examination was applied according to regular procedures. The ethical approval of using human heart samples was obtained from the Research Ethics Committee of Xinqiao Hospital, Chongqing, China, and written informed consent was obtained from each patient.

2.2. *In vitro* transcription of Cas9 mRNA and Guide RNAs

Cas9 mRNA was transcribed *in vitro* with mMESSAGE mMACHINE® T7 Ultra Kit (Ambion®). Guide RNAs (gRNA 1#: TGCCTGATCATCATCAGGG with PAM motif TGG; gRNA 2#: CCTAGGACCTTACTTCTT with PAM motif AGG) targeting intron 8 and intron 9 were transcribed with MEGAscript™ Kit (Ambion®). Transcribed products were purified with MEGAclear™ Kit (Ambion®). Donor vector was constructed by In-Fusion cloning, containing 3 kb 5' homology arm, 1.7 kb CDS (mutated exon 9 was fused to cDNA cloning exon 10 to exon 19) and 3 kb 3' homology arm.

2.3. Generation of the MAP4 (S667A, S737E and S760E) knock in (MAP4 KI) mice

The MAP4 KI mice were constructed and identified by the Shanghai Biomodel Organism Science & Technology Development Co., Ltd. Cas9 mRNA, Guide RNAs and donor vector were microinjected into fertilized eggs (C57BL/6J), before the eggs were implanted into surrogate C57BL/6J females. Mouse genotyping was determined by polymerase chain reaction with the primers: 5'-ACCTTTAGGAGTATCCCG-3', 5'-TTCAAG

CAATAGCAGCAGA-3' and 5'-TGTAATTGGCTTTGGCTTCAC-3' were used for genotyping. WT and targeted alleles resulted in bands of 184 bp and 347 bp, respectively.

2.4. Animal studies

MAP 4 KI mice were backcrossed to a C57BL/6J genetic background for more than ten generations. Male or female WT littermates were used as controls for experiments with corresponded MAP4 KI male or female mice. The age of mice ranged from 10 to 74 weeks (10–14 weeks, 30–34 weeks and 70–74 weeks), and the corresponded weights of them were 22–26 g, 25–30 g and 28–33 g, respectively. The mice were anesthetized with pentobarbital sodium (1%, 50 mg/kg) by intraperitoneal injection. MI and TAC mouse models were induced by open-chest surgery in C57BL/6 J mice (10–14 weeks) as previously described [18,19]. The MI mice (n = 5 animals/group) were sacrificed at 0 min, 5 min, 60 min and 360 min after ligation and the TAC mice (n = 6 animals/group) were sacrificed after three weeks of surgery, left ventricular (LV) free wall tissues of these models were used for experiments. Experiments involving animals were performed in accordance with United Kingdom Home Office and European Union guidelines and were approved by the Animal Care Centre of the Third Military Medical University (Army Medical University).

2.5. Primary cell culture

Neonatal mouse cardiomyocytes were prepared as described [18]. Briefly, neonatal cardiomyocytes were isolated by enzymatic disassociation of 1-day-old neonatal mouse hearts. Cardiomyocytes were plated for 2 h to remove fibroblasts. Cells were then plated on 1% gelatincoated plates in medium containing 10% horse serum and 5% fetal calf serum, and 0.1 mM bromodeoxyuridine was applied to inhibit fibroblasts proliferation. Eighteen hours after plating, cells were changed into serum-free medium. For neonatal mouse cardiac fibroblasts, cells were isolated using the crude method of collagenase type II enzymatic digestion, final cell suspension including cardiomyocytes and fibroblasts was separated by allowing the cell suspension to sediment in an uncoated culture dish at 37 °C for 1 h. Pre-plating facilitates fibroblasts to adhere to the culture dish separating cardiomyocytes floating in the suspension, fibroblasts were cultured in Dulbecco's modified Eagle's medium with 10% fetal bovine serum [20]. The cells were then used for experiments as stated. After transfection of adenovirus overexpressing MAP4(Ala) or CMV-null for 36 h, then isoprenaline (ISO) (Sigma-Aldrich Cat# 15627, 20 uM) was applied to stimulate cells for 48 h. During the stimulation, SB203580 (Calbiochem Cat# 559389, 5 μM) was applied to pretreat the cells for 1 h before ISO treatment as required. The in vitro experiments were conducted 5 times independently.

2.6. Extraction and quantification of tubulin fractions

The free and polymerized tubulin fractions of LV heart tissue were isolated using a method previously described [10,21]. Briefly, fresh LV heart tissues were homogenized in 1 ml of microtubule stabilization buffer (0.1 M piperazine-N,N'-bis (2-ethanesulfonic acid, pH 6.8) (PIPES), 2 mM ethylene glycol-bis (β-aminoethylether)-N,N,N',N'-tetraacetic acid (EGTA), 2 mM ethylenediaminetetraacetic acid (EDTA), 0.5 mM MgCl₂, 20% glycerol) with 0.1% Triton X-100, and centrifuged at 100,000g at 25 °C for 15 min. The supernatants were saved as the free tubulin fractions, and the pellets were resuspended at 0 °C in 1 ml of lysis buffer; after 1 h at 0 °C, they were centrifuged at 100,000g at 4 °C for 15 min, and the supernatants were saved as the polymerized tubulin fractions. The free and polymerized tubulin fractions of cells were isolated as our previous study described [9]. Briefly, cells were washed twice with microtubule stabilization buffer, and incubated with microtubule stabilization buffer with 0.1% Triton X-100 for 30 min, and then centrifuged at 15,000 rpm for 5 min, the supernatants

collected as the free tubulin fraction. The insoluble fraction, corresponding to the polymerized tubulin, was then solubilized in a RIPA lysis buffer. Protease inhibitors were used throughout. The polymerized and free tubulin fractions were quantified using Western blot (WB) analysis.

2.7. Mitochondria fractions preparation

Mitochondrial fractions were prepared and validated from LV cardiac tissues or cardiomyocytes according to the method previously described [13,22]. Briefly, LV heart tissues or cells were quickly collected in ice-cold phosphate buffer saline (PBS) and homogenized in ice-cold mitochondria isolation buffer (MIB: 310 mM sucrose, 20 mM Tris-HCl, 1 mM EGTA, pH 7.2). Mitochondria were purified by differential centrifugation: 1200g at 4 °C for 10 min, and then the supernatant was collected and again centrifuged at 12,000g, 4 °C for 10 min to form a crude mitochondrial pellet.

2.8. Immunoblotting analysis

Right ventricle myocardium of patients with TOF and LV myocardium of C57BL/6J mice were dissected and homogenized in a tissue protein extraction reagent (T-PER, Thermo Scientific). Cell samples were homogenized in RIPA buffer (Sigma-Aldrich Product Number R0278) with protease inhibitor tablets. The lysate was centrifuged at 16,000g, 4 °C for 15 min to remove insoluble protein. SDS-PAGE was carried out after equal BCA-based protein loading for each sample using gradient gels. Separated proteins were transferred to PVDF membranes (Millipore), blocked with 5% skimmed milk, and then incubated at 4 °C overnight with the corresponding primary antibodies and the secondary antibody in sequence. Specific protein bands were detected using avidinbiotinylated horseradish peroxidase in conjunction with an enhanced chemiluminescence detection kit (GE Healthcare). The following antibodies were used in this experiment: p38 MAPK (Cell Signaling Technology Cat# 9212, RRID:AB_330713, 1:1000), Phospho-p38 MAPK (p-P38) (Cell Signaling Technology Cat# 9211, RRID:AB_331641, 1:1000), VDAC (Cell Signaling Technology Cat# 4661, RRID:AB_10557420, 1:3000), Cleaved Caspase-3 (Cell Signaling Technology Cat# 9661, RRID:AB_2341188, 1:1000), Caspase-3 (Cell Signaling Technology Cat# 9662, RRID:AB_331439, 1:2000), GAPDH (Proteintech Group Cat# 60004-1-Ig, RRID:AB_2107436, 1:5000), p-MAP4 (S768) (Biologend Cat# 621102, 1:5000), and rabbit polyclonal antibody against p-MAP4 (S696) (GL Biochem, 1:1000), p-MAP4 (S787) (GL Biochem, 1:1000) or polyclonal antibody against p-MAP4 (S737) (GL Biochem, 1:1000), α-tubulin (Proteintech Group Cat# 11224-1-AP, RRID:AB_2210206, 1:2000), cytochrome c (Santa Cruz Biotechnology Cat# sc-13156, RRID:AB_627385, 1:5000), ANP (Santa Cruz Biotechnology Cat# sc-515701, 1:1000), BNP (Santa Cruz Biotechnology Cat# sc-271185, RRID:AB_10609757, 1:1000), MYH7 (Santa Cruz Biotechnology Cat# sc-53089, RRID:AB_2147281, 1:1000), COL1A1 (Santa Cruz Biotechnology Cat# sc-293182, 1:1000), COL1A2 (Santa Cruz Biotechnology Cat# sc-393537, 1:1000), COL3A1 (Santa Cruz Biotechnology Cat# sc-271249, RRID:AB_10613985, 1:1000), RIP3 (Santa Cruz Biotechnology Cat# sc-374639, RRID:AB_10992232, 1:2000), p-MLKL (Abcam Cat# ab196436, RRID:AB_2687465, 1:1000), MLKL (Abcam Cat# ab194699, 1:2000), FN (Abcam Cat# ab2413, RRID:AB_2262874, 1:5000), α-SMA (Abcam Cat# ab5649, 1:4000), MAP4 (Bethyl Cat# A301-489A, RRID:AB_999616, 1:1000), E-cadherin (Cell Signaling Technology Cat# 3195, RRID:AB_2291471, 1:2000), Calnexin (Abcam Cat# ab22595, RRID:AB_2069006, 1:4000), Histone H3 (Bioss Inc. Cat# bs-0349R-HRP, RRID:AB_11112443, 1:1000), transcription factor GATA-4 (GATA4) (Abcam Cat# ab84593, RRID:AB_10670538, 1:2000). Rabbit polyclonal antibodies against p-MAP4 (S696), p-MAP4 (S787) and p-MAP4 (S737) were raised in house using the C-terminal 14 amino acids (PNKEPPP(pS)PEKKAK, KVAEKRT(pS)PSKPSSA, RP(pS) TLPARDVKKPK and the respective non-phosphorylated peptides)

conjugated to bovine serum albumin (BSA). The antibodies made in-house were validated (Fig. S8).

2.9. Site-directed mutagenesis of MAP4 and MKK6 recombinant adenovirus construction and transduction

Primers were designed to generate point mutations of MAP4 (S768A and S787A) through polymerase chain reaction reactions using the QuikChange® Multi Site-Directed Mutagenesis Kit, and MKK6(Glu) adenovirus was constructed as previously described [9,13].

2.10. Electron microscopy

LV myocardium or cardiomyocytes were fixed in 2.5% glutaraldehyde followed by dehydration, vibratome sliced and recut on a microtome and stained with uranyl acetate and lead citrate overnight. The sections were examined using a transmission electron microscope (TEM) (TECNAL-12, Philips).

2.11. Immunofluorescence

The cardiomyocytes were fixed in 4% paraformaldehyde for 10 min, permeabilized with 0.1% Triton X-100 in PBS for 10 min, and blocked in 3% BSA for 0.5 h. To obtain the MT structure, rabbit anti- α -tubulin primary antibodies (Proteintech Group Cat# 11224-1-AP, RRID: AB_2210206, 1:50) were diluted with PBS, and the coverslips were incubated at 4 °C overnight. The coverslips were washed in PBS and then incubated with goat anti-rabbit secondary antibodies conjugated to fluorescein isothiocyanate (FITC) for 1 h at 37 °C. The nuclei were then stained for 2 min with 4', 6-diamidino-2-phenylindole (DAPI) (Sigma-Aldrich, 0.5 μ g/ml). While for cardiac troponin I (cTnI) (Proteintech Group Cat# 21652-1-AP, 1:50) and FITC-wheat germ agglutinins (WGA) (Sigma, Cat# L4895, 20 μ g/ml) or terminal deoxynucleotidyl transferase-mediated dUTP nick-end labeling (TUNEL) co-staining, the cells were incubated with cTnI at 4 °C overnight and then co-incubated with secondary antibodies conjugated to Cy3 and FITC-WGA or fluorescein-TUNEL reaction mixture for 1 h at 37 °C, and then the nuclei were stained for 2 min with DAPI. The cells were imaged using confocal microscopy (TCS-NT, Leica). Cell cross sectional area was assessed using an Image J software according to the known distance and pixels conversion.

2.12. Histological analysis

The heart tissue was cut and fixed with 10% formalin, embedded in paraffin, and sectioned at 6- μ m thickness. The sections were incubated in 3% H₂O₂ in methanol to prevent endogenous peroxidation and blocked with 3% BSA in PBS. For routine histopathology, LV or whole heart sections were stained with haematoxylin-eosin. For analysis of cardiomyocyte cross sectional area, the LV heart sections were stained with FITC-WGA as previously described [23]. For analysis of fibrosis, LV heart sections were stained with Masson's trichrome. And the analysis of α -SMA was stained by anti- α -SMA antibody.

2.13. Immunoprecipitation

To discern the protein interaction between MAP4 and tubulin, LV heart tissues were lysed in RIPA buffer with a protease inhibitor tablets. The α -tubulin (Santa Cruz Biotechnology Cat# sc-8035, RRID: AB_628408) antibody was incubated with cell lysate for 6 h at 4 °C, then the complexes were precipitated with protein A/G-Sepharose (Santa Cruz Biotechnology Cat# sc-2003, RRID:AB_10201400) overnight at 4 °C. The precipitates were washed 5 times with PBS at 0 °C and separated by SDS-PAGE and probed by rabbit anti-MAP4 antibody using WB.

2.14. Apoptosis assay

In Situ Cell Death Detection Kit and In Situ Cell Death Detection Kit, Fluorescein (Roche, Cat# 11684795910) were used for apoptosis assay of deparaffinized LV heart tissue sections or cardiomyocytes. Images of each group were randomly chosen using a BX61 Olympus microscope or confocal microscopy and further analyzed by Image pro plus 5 software.

2.15. Echocardiography and blood pressure analysis

Mice were anesthetized with a mixture of isoflurane and oxygen. Hypertrophy was assessed by echocardiography with a Vivid 7 (GE Medical Systems) instrument. The images were collected from the view of typical parasternal long-axis, apical four-chamber and apical five-chamber. GE Medical Systems software was used for data acquisition and subsequent analysis. Blood pressure analysis was performed using the non-invasive tail cuff method (BP-98A, Softron Biotechnology).

2.16. Blood parameters

Blood samples were collected by retro-orbital puncture from anesthetized animals. Serum levels of creatinine (Cr), alkaline phosphatase (ALP), total cholesterol (Tch), high density lipoprotein cholesterol (HDL-C), low density lipoprotein cholesterol (LDL-C), triglyceride (TG), urea nitrogen (UN), alanine aminotransferase (ALT), cardiac troponin T (cTnT) and creatine kinase-MB (CK-MB) were determined using commercial kits after fasting 8–12 h. Random blood glucose (RBG) (measured at random time) and fasting blood glucose (FBG) (measured after fasting 8–12 h) was monitored using blood glucose strips and the glucometer.

2.17. Statistical analysis

Data represent mean \pm SEM. The data meet the assumptions of the tests. Statistical differences between groups were assessed by two-tailed Student's *t*-test or one-way analysis of variance (ANOVA) post hoc tests, as appropriate. In experiment of patients, the data were analyzed by non-parametric Mann-Whitney test and expressed as medians and quartile ranges. For all studies, values of *P* < 0.05 were considered statistically significant. Statistical analysis was performed with the software program IBM SPSS STATISTIC, version 22 (SPSS Inc), and PASS 11 (NCSS Inc) was used to calculate the sample size of the experiments by one way ANOVA power analysis or two-sample *t*-test power analysis.

3. Results

3.1. Cardiac MAP4 hyperphosphorylation in hypoxic and pressure overload cardiomyopathy

We found that MAP4 phosphorylation was increased in cultured cardiomyocytes exposed to hypoxia [10,13]. To elucidate the general pathophysiological relevance, we examined the changes of MAP4 phosphorylation in heart tissues from patients with TOF (Fig. 1a and b). TOF is a congenital heart defect involving four anatomical abnormalities of the heart, which result in low blood oxygenation due to the mixing of oxygenated and deoxygenated blood in the left ventricle via ventricular septal defect [24]. Using WB analysis, we observed markedly increased phosphorylation levels of MAP4 at S768 and S787 but little distinction at S696 in cardiac tissues from hypoxemic patients when compared with those in patients with normoxemia (Fig. 1a and b, Table S2). Considering the co-existence of hypoxia and hypertrophy in these specimens, cardiac MAP4 phosphorylation (S667, S737 and S760, corresponding to the S696, S768 and S787 respectively in human) was

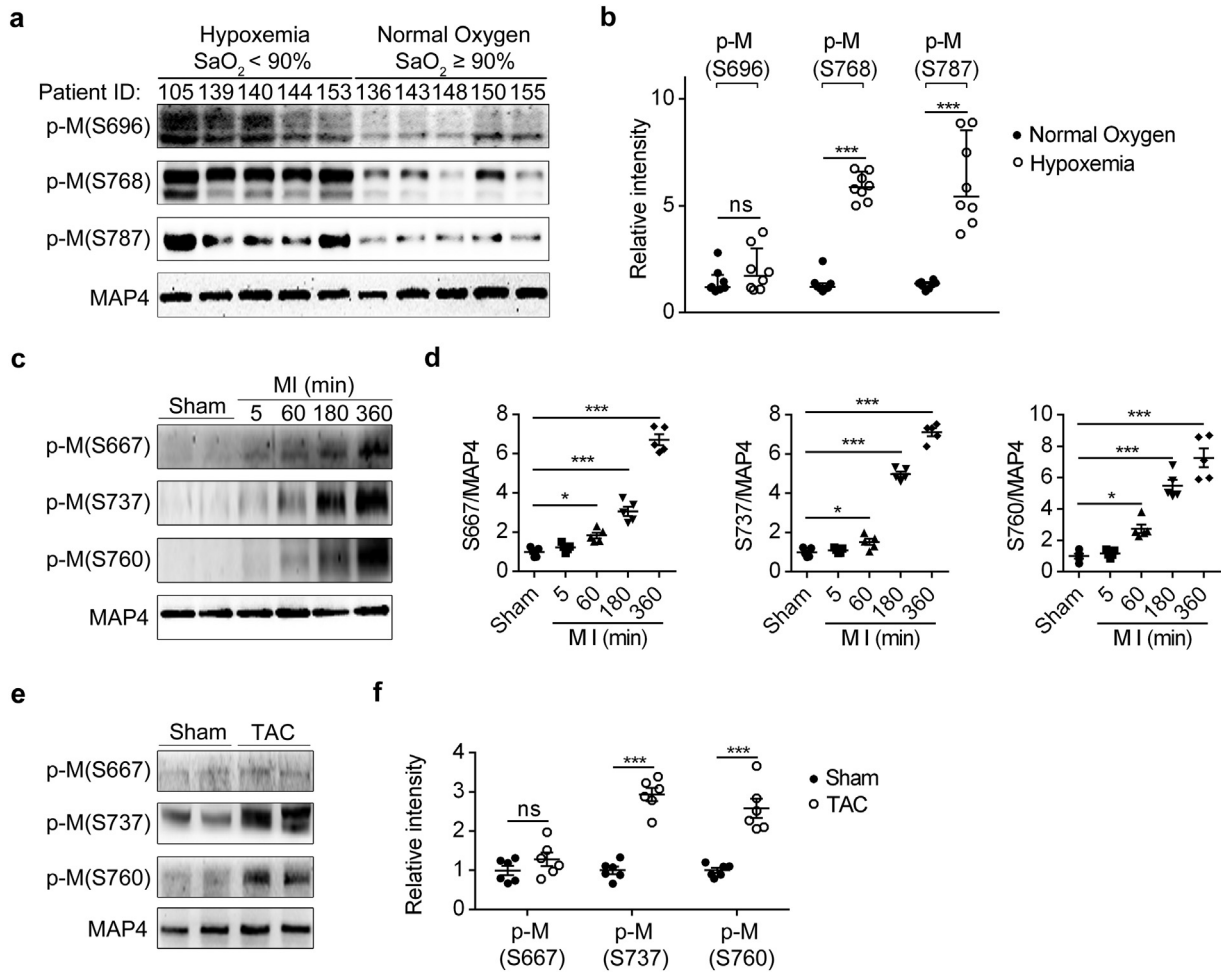


Fig. 1. Cardiac MAP4 hyperphosphorylation in hypoxic and pressure overload cardiomyopathy. (a, b) Representative WB (a) and quantitative analysis (b) depicting p-M (S696, S768 and S787) in TOF patients with hypoxemia. Data showed median (interquartile range). $n = 8$. (c, d) MAP4 phosphorylation was examined following MI at 0 min, 5 min, 60 min, 180 min and 360 min. $n = 5$. (e, f) WB analysis exhibited p-M (S667, S737 and S760) in mice with TAC for three weeks. $n = 6$. p-M, p-MAP4. The graph showed mean \pm SEM (d and f). * $P < 0.05$, **** $P < 0.001$, ns, not statistically significant. P values were derived from non-parametric Mann-Whitney test (b), two-tailed Student's t -test (f) and one-way ANOVA with Bonferroni's post-test (d).

detected in mice with MI (Fig. 1c and d) or TAC (Fig. 1e and f). In both mouse models, MAP4 phosphorylation (S737 and S760) displayed a robust rise while phosphorylation of S667 just increased in the MI models, accompanied with intense activation of p38/MAPK pathway (Fig. S1A–D). Thus, the changes under MI and TAC pathological conditions further revealed a universal rise in cardiac MAP4 phosphorylation (S737 and S760). In addition, in keeping with our previous studies [10], p38/MAPK is identified to be the upstream signaling responsible for MAP4 phosphorylation *in vivo*.

3.2. Genetic mutations of phosphorylation sites of MAP4

The amino acid residues S696, S768 and S787 of human MAP4 are the critical sites responsible for MAP4 binding to tubulin, and phosphorylation of these sites lead to tubulin depolymerization [10,15,16]. Importantly, in cultured neonatal rat cardiomyocytes, p-MAP4 detached from tubulin could translocate from the cytosol to mitochondria leading to mitochondrial permeability transition pore opening and mitochondrial apoptosis [13]. And the earlier results indicated that MAP4 phosphorylation (S737 and S760) were robust increased in various pathological conditions. To elucidate the physiological function of those phosphorylation sites of MAP4 *in vivo*, we generated mouse strain that mimicked the phosphorylated form of MAP4 at S737 and S760, with unphosphorylated S667. The technique of clustered regularly interspaced short palindromic repeats-associated protein 9 was adopted to knock in

the coding sequence of A667, E737 and E760 in the ninth exon of MAP4 gene by homologous recombination to replace the sequence of S667, S737 and S760 (Fig. 2a). Polymerase chain reaction (Fig. 2b) and WB (Fig. 2c and d) were applied to identify the MAP4 KI mice.

3.3. MAP4 phosphorylation induces pathological cardiac hypertrophy

The blood biochemical and metabolism parameters were examined to investigate whether the remote organs may involve the regulation of cardiac phenotype through humoral system, and there were no significant differences between wild type (WT) and MAP4 KI mice at 70–74 weeks of age (Table S3). In addition, body weight was comparable between the two genotypes of mice within the age range studied (6 to 74 weeks) (Fig. S2). However, there was an age-dependent increase in absolute whole heart weight or heart weight normalized by body weight or by tibia length in MAP4 KI mice by 22%, 19% and 23%, respectively at 30–34 weeks of age, and by 32%, 31% and 33% at 70–74 weeks of age while being comparable between the genotypes at 10–14 weeks of age (Fig. 3a, b and c). A pronounced thickening of the interventricular septum (IVS) and the ventricular wall was observed from 30 to 74 weeks with histological analysis (Fig. 3d).

Cardiac morphology and function were analyzed using echocardiography (Table 1). Thickness of end-diastolic and end-systolic IVS and the LV posterior wall as well as LV myocardial mass, were significantly and age-dependently greater in MAP4 KI than in WT littermates (Table 1).

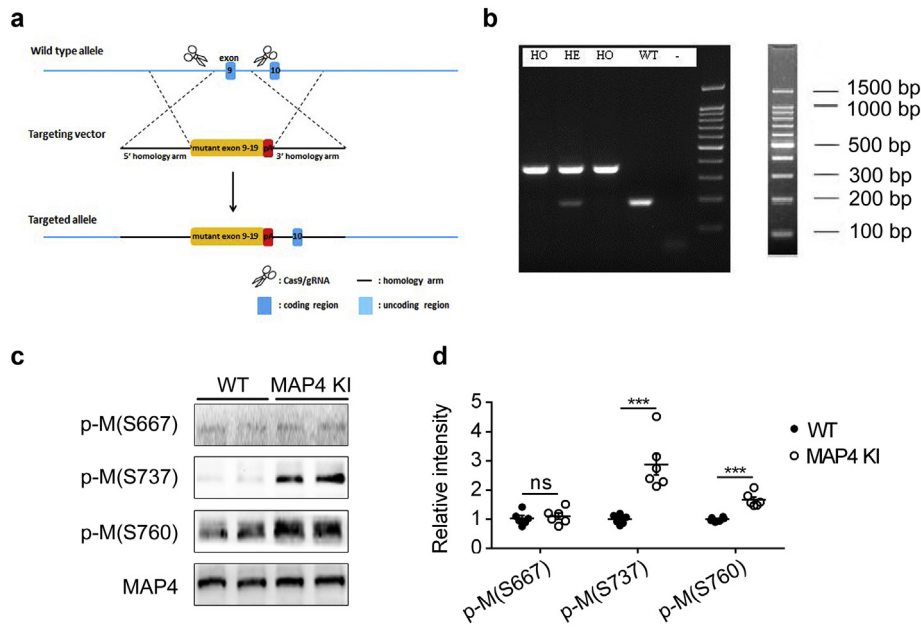


Fig. 2. Genetic mutations of phosphorylation sites of MAP4. (a) Schematic of MAP4 KI mice. CRISPR/Cas9 technique was used to generate mouse strain with mutated MAP4 by knocking in the coding sequence (S667A, S737E and S760E) in the ninth exon of MAP4 gene by homologous recombination. CRISPR/Cas9, clustered regularly interspaced short palindromic repeats-associated protein 9. (b) Representative polymerase chain reaction identification showing the HO, HE and WT genotype mice. HO, homozygote; HE, heterozygote. (c, d) Representative WB (c) and quantitative analysis (d) showing phosphorylation of MAP4 in MAP4 KI mice aged at 10 to 14 weeks. The graph showed the mean \pm SEM ($n = 6$). *** $P < 0.001$, ns, not statistically significant. P values were derived from two-tailed Student's t -test.

Cardiac systolic and diastolic functions were comparable at the age of 10–14 weeks. At the age of 30–34 weeks, cardiac diastolic dysfunction was firstly detected in MAP4 KI mice, as indicated by decreased mitral E velocity, increased deceleration time of mitral inflow E and decreased peak E wave of early diastolic at septal annulus relative to peak A wave of late diastolic septal annulus. By the age of 70–74 weeks, diastolic dysfunction further worsened and was accompanied by systolic dysfunction, as manifested by suppressed LV ejection fraction, fractional shortening and velocity of circumferential fiber shortening (Table 1).

Besides, immunostaining with FITC-conjugated WGA was applied to quantify the LV cardiomyocyte size. While little distinction was observed at the age of 10–14 weeks, cardiomyocytes of MAP4 KI mice exhibited increased cross section area by 23% at 30–34 weeks of age and by 47% at 70–74 weeks of age compared with age-matched WT littermates (Fig. 3e and f). Up-regulation of protein markers of myocardial hypertrophy, including atrial natriuretic peptide and myosin heavy chain 7, was detected in MAP4 KI mice at 30–34 and 70–74 weeks of age, but not at 10–14 weeks versus respective WT littermates (Fig. 3g and h). Blood levels of cTnT and CK-MB, markers of cardiac damage, displayed little changes between the genotypes (Fig. 3i).

The ultrastructure of heart was further observed by TEM. At 10–14 weeks of age, myofilament exhibited similar appearance between genotypes, while the myofilament dissolution and sparseness were evident in MAP4 KI mice aged at 30–34 and 70–74 weeks (Fig. 3j).

To further assess the effects of MAP4 phosphorylation on cardiac hypertrophy in vitro, primary neonatal mouse cardiomyocytes were treated with ISO. An overexpression adenovirus encoding human MAP4(Ala), in which the serine at 768 and 787 was altered to alanine (Ala) to mimic the nonphosphorylated form of MAP4 (Fig. S7), was generated [13]. The markers of cardiac hypertrophy, e.g. atrial natriuretic peptide, brain natriuretic peptide and myosin heavy chain 7, were all increased in response to treatment with ISO in cardiomyocytes, which was abrogated by transfection of MAP4(Ala) adenovirus (Fig. 3k and l). In addition, MAP4(Ala) overexpression was also found to reduce the cross section area of neonatal mouse cardiomyocytes under ISO treatment (Fig. 3m).

Last but not least, little differences were noted in blood pressure at the age of 30–34 and 70–74 weeks (Table 2). Thus, the functional,

histocytological and pathological observations strongly indicated that MAP4 phosphorylation promoted pathological cardiac hypertrophy in vivo and in vitro, the effect of which occurred independent of hypertension.

3.4. The effect of MAP4 phosphorylation on cardiomyocytes apoptosis

We previously demonstrated that MAP4 phosphorylation was a modulator of apoptosis in hypoxic neonatal cardiomyocytes in vitro [13]. To validate this notion in vivo, LV heart tissues of 10–14 and 70–74 week-old MAP4 KI mice were examined. There was a 1.81- and 2.45-fold increase in cleaved caspase-3 protein levels in hearts of both 10–14 and 70–74 week-old MAP4 KI versus WT littermates (Fig. 4a and b), supporting activation of caspase-dependent apoptotic pathway that proceeded to the onset of other pathologies. This notion was further supported by TUNEL staining showing a marked increase in TUNEL-positive stained cardiomyocytes in MAP4 KI mice hearts both at the age of 10–14 and 70–74 weeks versus WT littermates (Fig. 4c and d). To test potential changes in cardiac cell necroptosis and necrosis, we determined protein levels of receptor-interacting protein kinase 3 and phosphor-mixed lineage kinase domain-like protein, as well as LV heart sections with haematoxylin-eosin staining, respectively, and found no difference between WT and MAP4 KI mice within the age range studied (10 to 74 weeks) (Fig. S3).

In order to elucidate the type of apoptosis, mitochondrial and non-mitochondrial fractions were isolated and validated from MAP4 KI and WT mice LV heart tissues, and analyzed using WB (Figs. S4a and 4e and f). Results suggested that cytochrome *c* in non-mitochondrial fractions was increased in MAP4 KI mice compared with WT littermates at 10–14 and 70–74 weeks of age (Fig. 4e and f), suggesting involvement of mitochondrial pathway for apoptosis. The alternation of mitochondrial morphology in MAP4 KI mice was further demonstrated by TEM examinations (Fig. 4g). At the age of 10–14 weeks, mitochondria of MAP4 KI mice exhibited moderate swelling and rarefaction of internal cristae. By 70–74 weeks of age, mitochondrial swelling and internal cristae destruction were aggravated, and mitochondrial visible vacuole and myelin-like structure could be noted. Meanwhile, classical

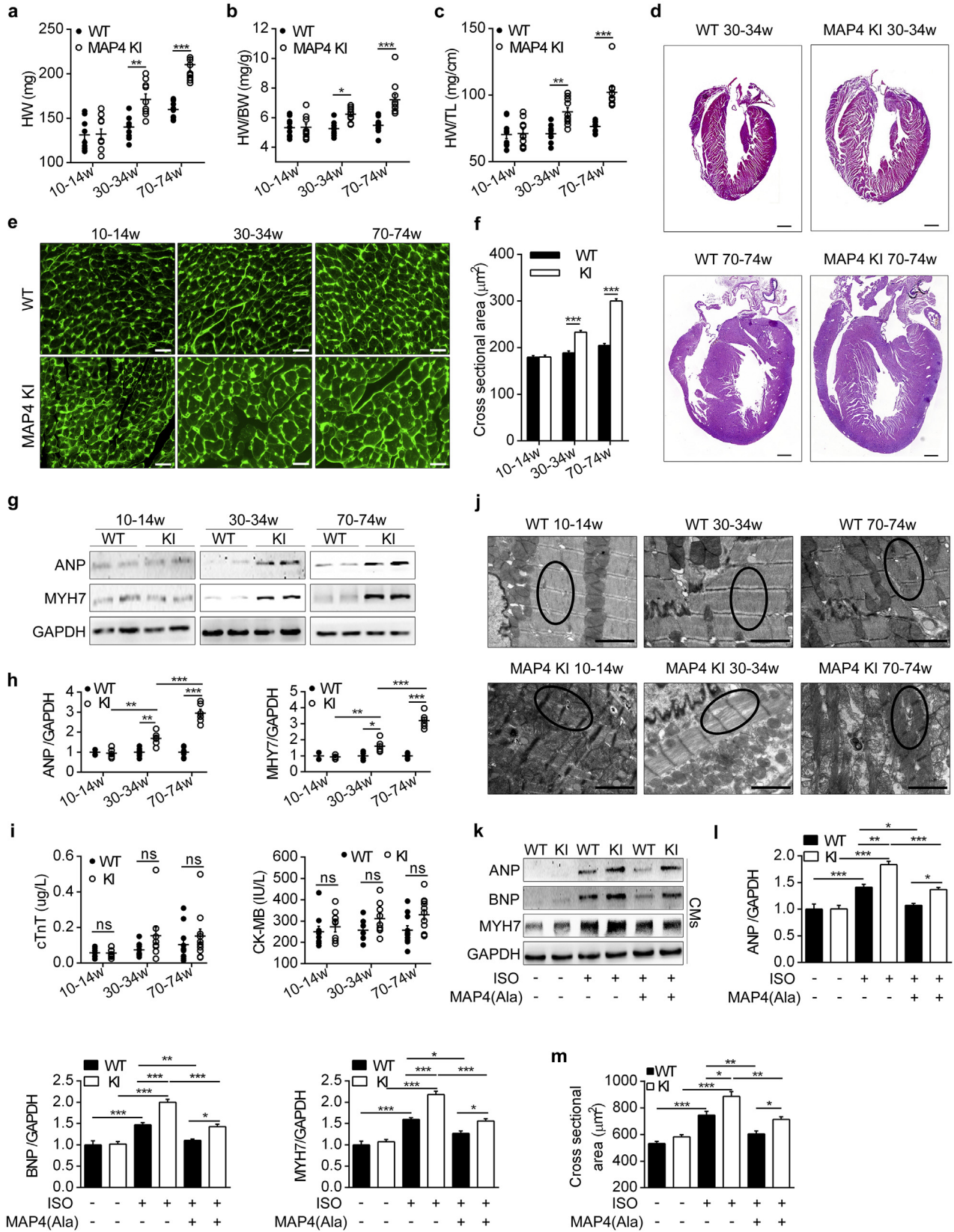


Fig. 3. MAP4 phosphorylation induces pathological cardiac hypertrophy. (a, b, c) Heart weight (HW), HW normalized by body weight (HW/BW) and HW normalized by tibia length (HW/TL) of two mouse models were determined. $n = 10$. (d) Heart histological sections with haematoxylin-eosin staining. Bar, 500 μm . $n = 6$. (e, f) FITC-WGA staining of LV heart sections, and cross sectional areas were analyzed in two mouse models. $n = 6$ (100 cells counted/animal). Bar, 20 μm . (g, h) Protein markers of hypertrophy in LV heart tissues were detected using WB analysis. $n = 6$. (i) Blood markers of cardiac damage from two mouse models were shown by cTnT and CK-MB. $n = 9-11$. (j) Representative TEM images showing ultrastructure of LV heart sarcomere (black circle represented myofilaments) between two mouse models. Bar, 2 μm . $n = 6$. (k, l) Protein markers of hypertrophy in CMs from two mouse models were detected with or without MAP4(Ala) transfection. $n = 5$. The experiment was conducted 5 times. (m) Cross sectional areas of CMs were analyzed by cTnT and FITC-WGA co-staining. $n = 5$. The experiment was conducted 5 times. ANP, atrial natriuretic peptide; MYH7, myosin heavy chain 7; BNP, brain natriuretic peptide; CMs, cardiomyocytes. Data were shown as mean \pm SEM. * $P < 0.05$, ** $P < 0.01$, *** $P < 0.001$, ns, not statistically significant. P values were derived from one-way ANOVA with Bonferroni's post-test.

Table 1
In vivo cardiac function of WT and MAP4 KI mice at different ages

	10–14w (n = 10/10)		30–34w (n = 11/11)		70–74w (n = 12/12)	
	WT	MAP4 KI	WT	MAP4 KI	WT	MAP4 KI
IVSs (mm)	1.09 ± 0.05	1.09 ± 0.05	1.16 ± 0.07	1.37 ± 0.07*	1.27 ± 0.06	1.57 ± 0.06 [†]
IVSd (mm)	0.84 ± 0.02	0.88 ± 0.04	0.84 ± 0.02	0.96 ± 0.03 [†]	0.93 ± 0.03	1.08 ± 0.02 [‡]
LVPWs (mm)	1.21 ± 0.07	1.26 ± 0.05	1.24 ± 0.06	1.44 ± 0.07*	1.34 ± 0.03	1.64 ± 0.05 [‡]
LVPWd (mm)	0.79 ± 0.02	0.83 ± 0.05	0.79 ± 0.03	1.01 ± 0.04 [‡]	0.91 ± 0.02	1.10 ± 0.03 [‡]
LVIDs (mm)	1.40 ± 0.09	1.49 ± 0.09	1.57 ± 0.11	1.61 ± 0.08	1.61 ± 0.10	1.98 ± 0.10 [‡]
LVIDd (mm)	3.10 ± 0.10	3.02 ± 0.10	3.15 ± 0.12	3.29 ± 0.09	3.35 ± 0.06	3.56 ± 0.05
EF (%)	90.75 ± 1.14	90.53 ± 1.00	88.69 ± 0.88	87.58 ± 1.32	86.36 ± 1.42	78.26 ± 0.83 [‡]
FS (%)	55.26 ± 2.01	54.60 ± 1.44	51.81 ± 1.14	50.88 ± 1.84	51.47 ± 1.94	42.28 ± 1.05 [‡]
Vcf (cir/s)	8.13 ± 0.41	7.16 ± 0.51	7.19 ± 0.50	6.84 ± 0.38	7.16 ± 0.44	5.94 ± 0.25*
E velocity (m/s)	0.63 ± 0.03	0.67 ± 0.03	0.67 ± 0.03	0.59 ± 0.03*	0.64 ± 0.02	0.53 ± 0.03 [†]
A velocity (m/s)	0.51 ± 0.03	0.56 ± 0.03	0.56 ± 0.02	0.50 ± 0.02	0.53 ± 0.02	0.52 ± 0.01
EDT (ms)	7.27 ± 0.60	8.63 ± 0.93	7.59 ± 0.44	10.01 ± 0.56 [†]	9.06 ± 0.41	12.20 ± 0.70 [‡]
E/A	1.24 ± 0.03	1.21 ± 0.02	1.21 ± 0.02	1.18 ± 0.02	1.22 ± 0.03	1.04 ± 0.06
Esa/Asa	1.34 ± 0.04	1.29 ± 0.06	1.33 ± 0.06	1.07 ± 0.05*	1.22 ± 0.03	0.71 ± 0.02 [‡]
IVRT (ms)	14.77 ± 1.72	15.45 ± 1.29	15.91 ± 1.24	19.09 ± 1.53	21.42 ± 1.24	28.12 ± 3.65
IVCT (ms)	16.70 ± 2.41	15.35 ± 1.58	14.39 ± 1.42	13.24 ± 1.08	17.72 ± 1.67	16.33 ± 1.85
Tei index	0.43 ± 0.06	0.39 ± 0.04	0.43 ± 0.04	0.44 ± 0.04	0.55 ± 0.04	0.62 ± 0.06
ET (ms)	75.13 ± 2.34	78.64 ± 1.92	72.22 ± 2.90	75.04 ± 1.66	71.61 ± 2.34	73.77 ± 1.92
LVMM (mg)	64.96 ± 3.45	67.23 ± 4.29	67.68 ± 5.23	93.81 ± 6.00 [‡]	86.79 ± 2.93	121.90 ± 3.58 [‡]

A velocity, Mitral A velocity; EF, ejection fraction; E velocity, Mitral E velocity; EDT, deceleration time of mitral inflow E; E/A, mitral E velocity relative to mitral A velocity; Esa/Asa, peak E wave of early diastolic at septal annulus relative to peak A wave of late diastolic septal annulus; ET, ejection time; FS, fractional shortening; IVSs, interventricular septal diameter at systole; IVSd, interventricular septal diameter at diastole; IVRT, intraventricular relaxation time; IVCT, intraventricular contraction time; LVPWs, LV posterior wall thickness at systole; LVPWd, LV posterior wall thickness at diastole; LVIDs, LV internal diameter at systole; LVIDd, LV internal diameter at diastole; LVMM, LV muscle mass; Vcf, velocity of circumferential fiber shortening. Data were shown as mean ± SEM (*P < 0.05, [†]P < 0.01, [‡]P < 0.001 vs. the corresponding WT group). P values were derived from one-way ANOVA with Bonferroni's post-test.

apoptotic morphology of cardiomyocytes was observed consistent with the increased TUNEL staining cardiomyocytes in MAP4 KI mice.

Finally, the correlation between MAP4 phosphorylation and apoptosis was further scrutinized in patients with TOF. Karyopyknosis, the classical morphological feature of apoptosis, was frequently observed in right ventricular myocardial tissues of hypoxemic patients (SaO₂ < 90%) as evidenced by light microscopy (Fig. S5A a, b, c and e) or TEM (Fig. S5B a, c and e), but not in tissues of patients with normoxemia (SaO₂ ≥ 90%) (Fig. S5A f–j and B f–j). This observation was consistent with a recent report showing an increased apoptotic activity in the myocardium from cyanotic, but not acyanotic TOF patients [25]. By TUNEL staining in situ, an apoptosis rate as high as 43.5% was detected in hypoxemic patients, a 4.0-fold increment over that in normoxemic patients (Fig. S5C and Table S1).

To confirm the consistency of the in vivo and in vitro findings regarding cardiomyocyte apoptosis, we examined apoptosis of primary cultured neonatal mouse cardiomyocytes of WT and MAP4 KI mice subjected to ISO treatment with or without MAP4(Ala) overexpression. Levels of cleaved caspase-3 and cardiomyocyte apoptosis were increased under baseline condition or with ISO challenge in MAP4 KI cardiomyocytes, which was attenuated by transfection with MAP4 (Ala) adenovirus (Fig. 4h, i, l and m). In addition, cytochrome c released in non-mitochondrial fractions in MAP4 KI cardiomyocytes was decreased following MAP4(Ala) transfection compared with cells transfected with CMV-null following ISO challenge (Figs. 4j, k and S4B). Furthermore, in cardiomyocytes prepared from WT and MAP4 KI neonatal mice, MAP4(Ala) transfection also protected against ISO-induced mitochondrial destructions as evaluated using TEM (Fig. 4n).

Table 2
In vivo blood pressure of WT and MAP4 KI mice at different ages.

	30–34w		70–74w	
	WT (n = 9)	KI (n = 13)	WT (n = 11)	KI (n = 12)
HR (bpm)	623 ± 15	638 ± 12	591 ± 12	563 ± 11
SBP (mmHg)	103 ± 2	103 ± 2	113 ± 1	110 ± 2
DBP (mmHg)	64 ± 1	67 ± 2	66 ± 1	68 ± 1
MBP (mmHg)	77 ± 1	79 ± 2	81 ± 1	82 ± 1

bpm, beat per minute; DBP, diastolic blood pressure; HR, heart rate; KI, MAP4 KI; MBP, mean blood pressure; SBP, systolic blood pressure. Data were shown as mean ± SEM. Statistics was done by one-way ANOVA.

Taken together, these data provided further evidence for a crucial role of MAP4 phosphorylation in cardiomyocyte apoptosis, prior to the onset of hypertrophy.

3.5. The effects of MAP4 phosphorylation on cardiac fibrosis

Pathological hypertrophy is closely associated with cardiac fibrosis [26,27]. We examined fibrotic markers that regulated turnover of extracellular matrix (ECM). There was no significant difference in these fibrotic parameters between WT and MAP4 KI mice at the age of 10–14 weeks (Fig. 5a–c). However, increased collagen deposition occurred in the perivascular area could be seen under TEM at the age of 30–34 and 70–74 weeks (Fig. 5a). Myocardial fibrotic area, detected by Masson's trichrome staining, was significantly increased in MAP4 KI mice at the age of 70–74 weeks (Fig. 5b and c). Protein levels of collagen 1A1, collagen1A2, collagen 3A1 and fibronectin, the primary ECM components in LV heart tissue, were robustly increased in MAP4 KI mice at the age of 30–34 and 70–74 weeks compared with WT littermates, while no change was observed at the age of 10–14 weeks (Fig. 5d and e). α -smooth muscle actin, a marker of fibrosis in non-cardiomyocyte, was analyzed using WB analysis and histochemical staining. Level of α -smooth muscle actin was comparable between WT and MAP4 KI mice of 10–14 week-old, but increased by 1.69- and 3.03-fold in MAP4 KI mice at 30–34 and 70–74 weeks, respectively (Fig. 5f and g), findings consistent with histochemical staining for α -smooth muscle actin (Fig. 5h and i).

Using the primary cultured neonatal mouse cardiac fibroblasts stimulated with ISO, we observed that MAP4(Ala) transfectants significantly reduced expression levels of collagen 1A1, collagen 1A2, collagen 3A1 and fibronectin of fibroblasts compared with CMV-null transfectants (Fig. 5j and k). Collectively, these in vivo and in vitro findings denoted an essential role for MAP4 phosphorylation in driving the progression of pathological cardiac fibrosis.

3.6. MAP4 phosphorylation induces MT disassembly and mitochondrial translocation of p-MAP4

The above results suggested that MAP4 phosphorylation promoted cardiomyocyte apoptosis in MAP4 KI mice as early as 10–14 weeks of age. Previous studies indicated that MAP4 phosphorylation not only

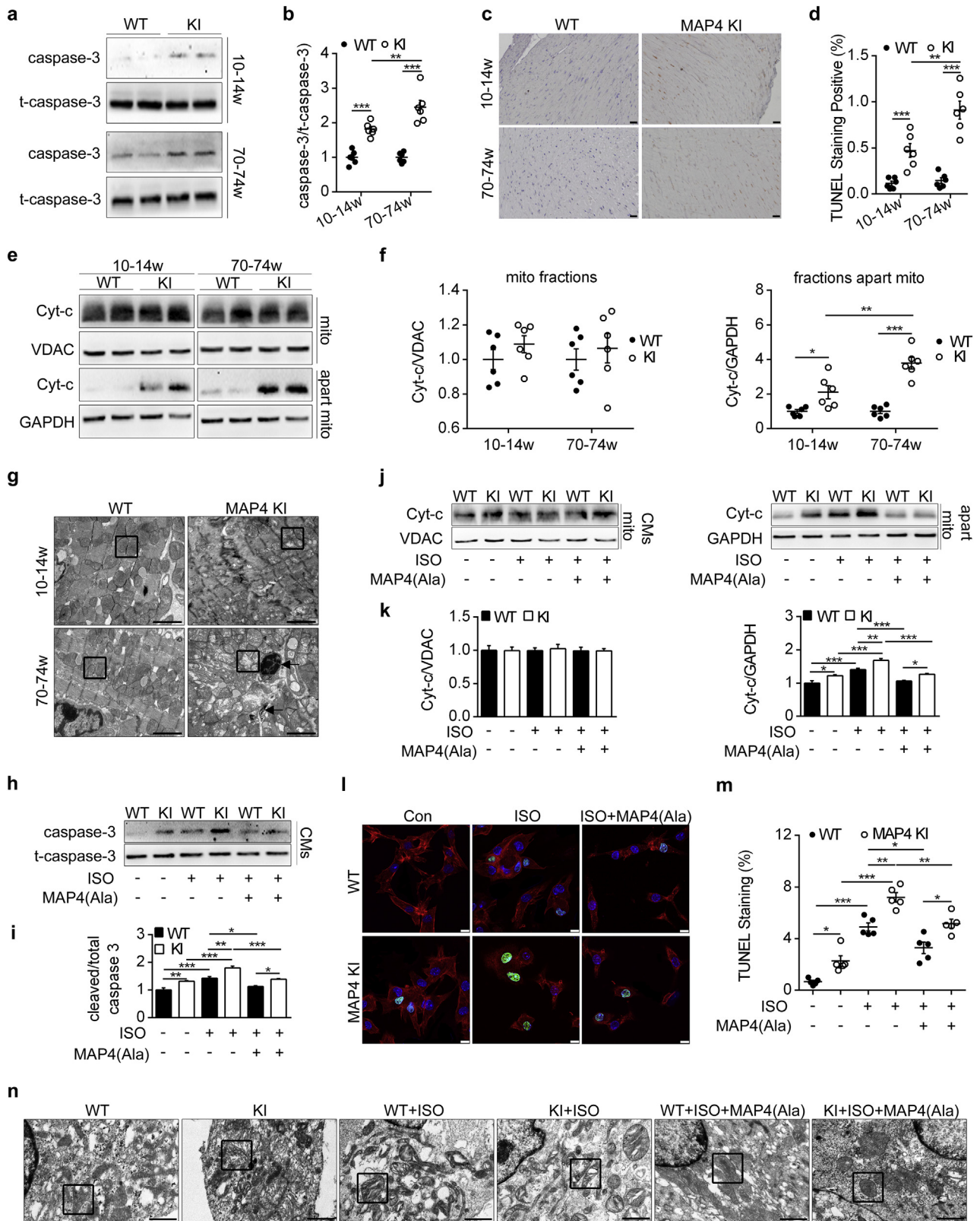


Fig. 4. The effect of MAP4 phosphorylation on cardiomyocyte apoptosis. (a, b) WB analysis displayed protein level of caspase-3 (cleaved) in two mouse models. $n = 6$. (c, d) Representative images and quantitative analysis depicted LV cardiac apoptosis using TUNEL staining. $n = 6$. (e, f) Detection of mitochondrial Cyt-c release by WB. $n = 6$. (g) Representative TEM images showing ultrastructure of CMs apoptosis and mitochondrial disruption (black square represented mitochondria, black arrows indicated chromatin margination and mitochondrial myelin-like structure). Bar, $2 \mu\text{m}$. $n = 6$. (h, i) Caspase-3 and t-caspase-3 in CMs from two mouse models with or without MAP4(Ala) were detected by WB. $n = 5$. The experiment was conducted 5 times. (j, k) Detection of mitochondrial Cyt-c release in CMs from two mouse models with or without MAP4(Ala) transfection. $n = 5$. The experiment was conducted 5 times. (l, m) Detection of CMs apoptosis by cTnI and fluorescein-TUNEL co-staining. Bar, $10 \mu\text{m}$. $n = 5$. The experiment was conducted 5 times. (n) Observation of CMs mitochondria with or without MAP4(Ala) transfection by TEM (Black square represented mitochondria). Bar, $1 \mu\text{m}$. The experiment was conducted 5 times. t-caspase-3, total caspase-3; Cyt-c, cytochrome c; mito, mitochondria. Data were shown as mean \pm SEM. * $P < 0.05$, ** $P < 0.01$, *** $P < 0.001$. P values were derived from one-way ANOVA with Bonferroni's post-test.

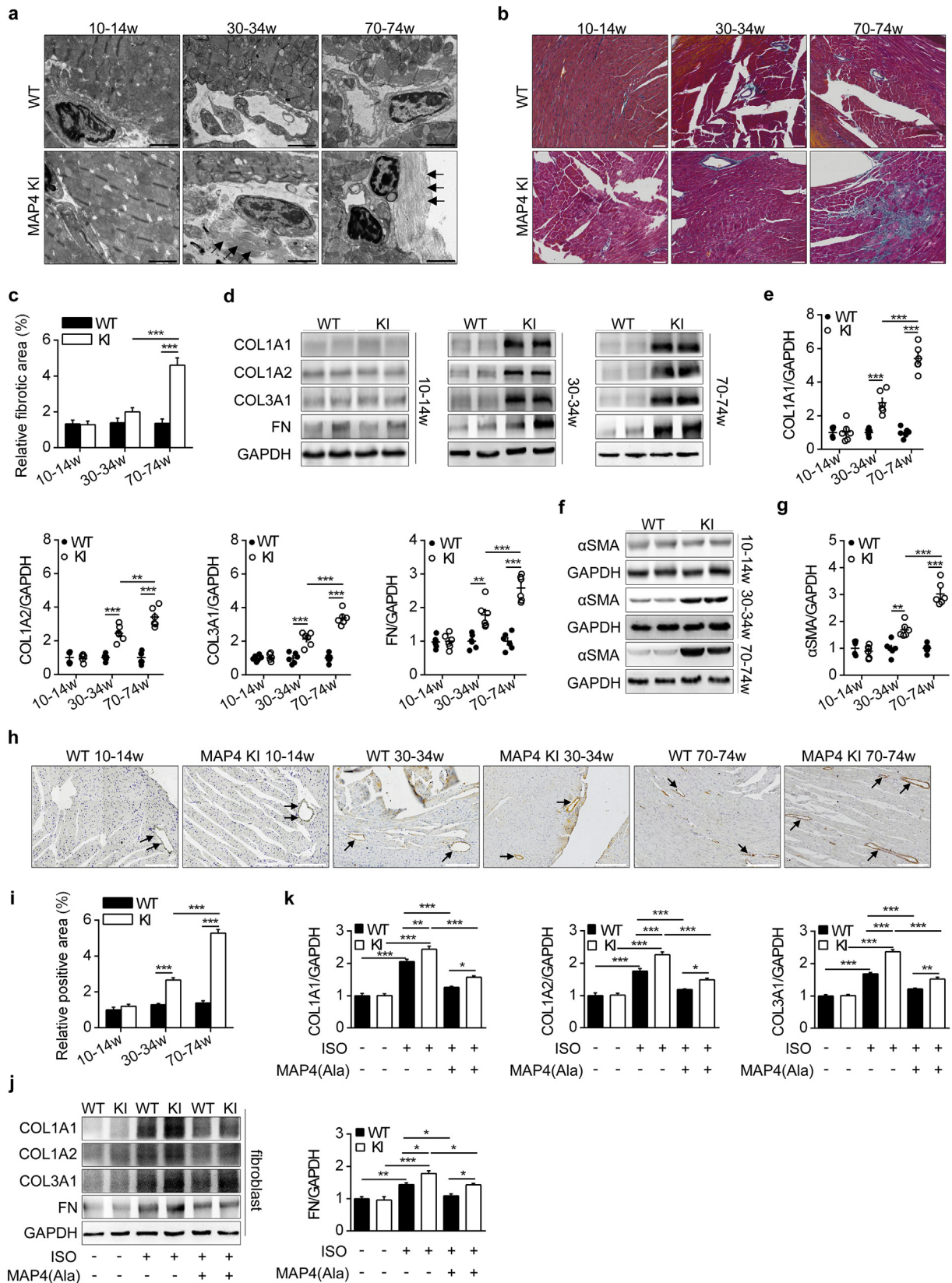


Fig. 5. The effects of MAP4 phosphorylation on cardiac fibrosis. (a) Representative TEM images showing ultrastructure of LV cardiac fibrosis (black arrows indicated collagenous fibers). Bar, 2 μ m. $n = 6$. (b, c) LV heart histological sections with Masson's trichrome staining in two mouse models. Bar, 50 μ m. $n = 6$. (d, e) WB analysis showing protein levels of collagen (COL) 1A1, 1A2, 3A1 and fibronectin (FN) in two mouse models. $n = 6$. (f, g) WB analysis showing protein levels of α -SMA in two mouse models. $n = 6$. (h, i) Detection of α -SMA by histochemical staining (black arrows indicated α -SMA) in the LV heart tissue of WT and MAP4 KI mice. Bar, 200 μ m. $n = 6$. (j, k) ECM protein markers were detected with or without MAP4(Ala) transfection in primary neonatal mouse myocardial fibroblasts. $n = 5$. The experiment was conducted 5 times. α -SMA, α -smooth muscle actin. Data were shown as mean \pm SEM. * $P < 0.05$, ** $P < 0.01$, *** $P < 0.001$. P values were derived from one-way ANOVA with Bonferroni's post-test.

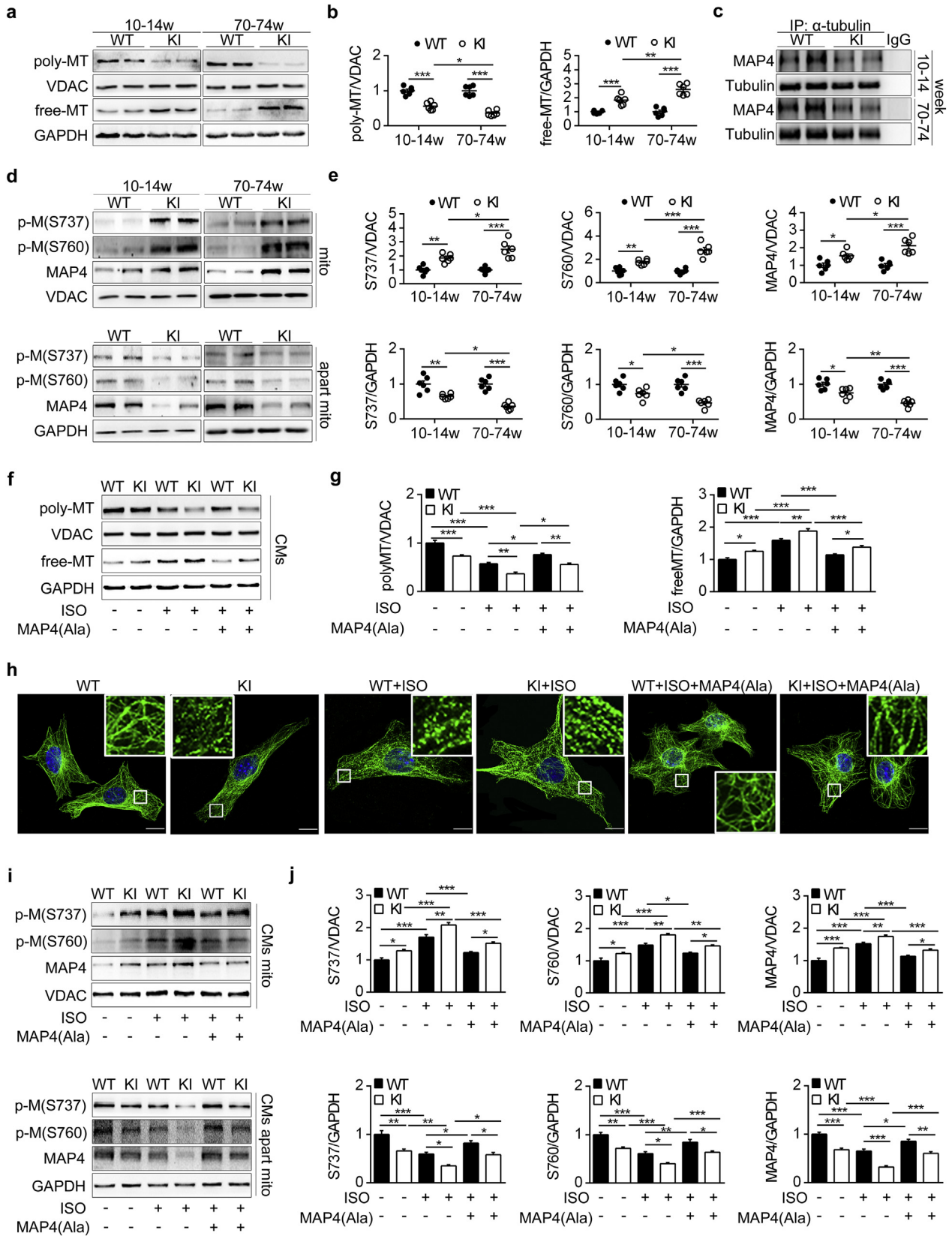
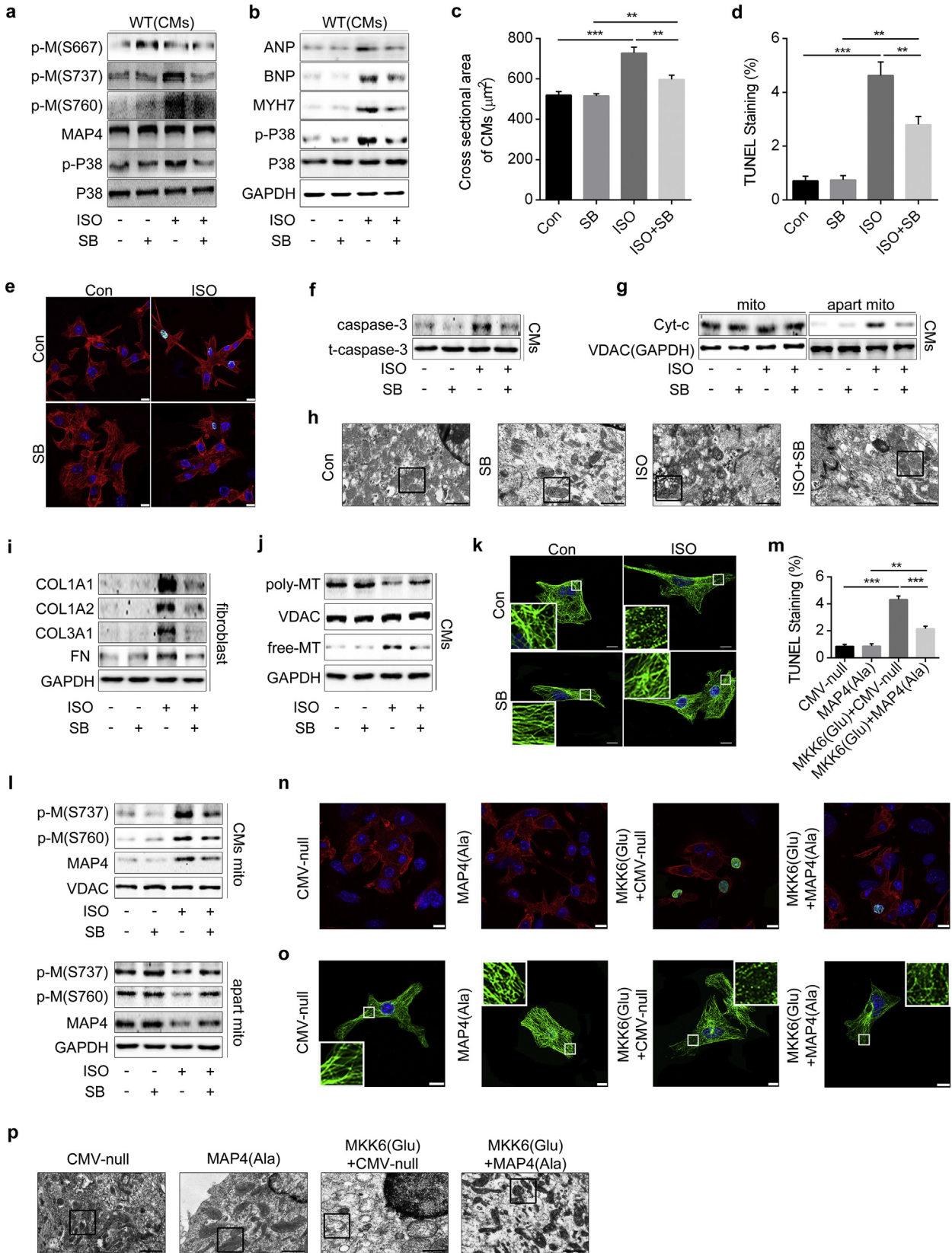


Fig. 6. MAP4 phosphorylation induces MT disassembly and mitochondrial translocation of p-MAP4. (a, b) WB analysis was used to detect polymerized (poly) or free tubulin in two mouse models. VDAC and GAPDH were used as the internal controls for poly and free tubulin, respectively. n = 6. (c) Determination of MAP4 binding to tubulin in two mouse models by immunoprecipitation (IP). n = 6. (d, e) WB analysis showing the levels of p-M in mitochondria fractions and fractions apart from mitochondria in two mouse models. n = 6. (f, g) Poly/free tubulin in CMs were detected by WB. n = 5. The experiment was conducted 5 times. (h) Representative confocal immunofluorescence images showing the MTs organization of the CMs. Bar, 10 μm. The inserts showed high magnification images of the representative MT network. (i, j) Detection of p-M translocation to mitochondria with or without MAP4(Ala) transfection in CMs. n = 5. The experiment was conducted 5 times. The Data were shown as mean ± SEM. *P < 0.05, **P < 0.01, ***P < 0.001. P values were derived from one-way ANOVA with Bonferroni's post-test.



led to MT disassembly, but also promoted mitochondrial translocation of p-MAP4, both of which favored apoptosis *in vitro* [10,13]. To confirm that this did occur *in vivo*, we studied MAP4 KI mice and observed a 1.79-fold decrease in polymerized tubulin with a parallel 1.83-fold increase in free tubulin compared with WT littermates (Fig. 6a and b), along with the dissociation of MAP4 from tubulin (Fig. 6c), indicative of MT disassembly. Meanwhile, p-MAP4 (S737 and S760) and total MAP4 in mitochondrial fractions of MAP4 KI mice also displayed a robust increase with a parallel decrease in the remaining non-mitochondrial fractions (Fig. 6d and e). These findings were consistent with our previous *in vitro* findings and confirmed p-MAP4 translocation from cytoplasm to mitochondria as a tentative mechanism of cardiac apoptosis in MAP4 KI mice. MT disassembly and mitochondrial translocation of p-MAP4 in MAP4 KI mice continued to the age at 70–74 weeks (Fig. 6a, b, d and e).

To explore whether the changes could be reversed by MAP4 dephosphorylation, we applied MAP4(Ala) adenovirus to the primary neonatal mouse cardiomyocytes subjected to ISO challenge. MAP4(Ala) overexpression promoted the tubulin polymerization with a parallel decrease in free-tubulin in response to ISO treatment (Fig. 6f and g). This notion was further supported by MT immunofluorescence staining of primary neonatal mouse cardiomyocyte, showing the protection of MT structure of MAP4(Ala) transfectants compared with cells transfected with CMV-null under ISO challenge (Fig. 6h). In addition, MAP4(Ala) transfection significantly decreased the mitochondrial translocation of p-MAP4 compared with CMV-null transfected cells (Fig. 6i and j).

3.7. Role of p38/MAPK activation in MAP4 phosphorylation-induced cardiac hypertrophy, apoptosis and fibrosis

Our earlier work suggested that MAP4 phosphorylation induced pathological cardiac hypertrophy, fibrosis and mitochondrial apoptosis, with p38/MAPK serving as an important kinase regulating MAP4 phosphorylation in hypoxic cardiomyocytes [10]. However, whether p38/MAPK signaling is involved in cardiac hypertrophy, apoptosis and fibrosis (and if this is mediated through MAP4 phosphorylation) remains unknown. We firstly studied whether p38/MAPK could regulate MAP4 phosphorylation under ISO treatment. Our data revealed that protein levels of p-MAP4 (S737 and S760) and p-P38 were increased after ISO stimulation, while p-MAP4 (S667), p38 and total MAP4 were kept unchanged. Conversely, the p38/MAPK inhibitor SB203580 inhibited p38/MAPK activation and MAP4 phosphorylation (S737 and S760) (Figs. 7a and S9A). The data suggested that p38/MAPK was pivotal upstream kinase that promoted MAP4 phosphorylation under ISO treatment.

We then observed the role of p38/MAPK in ISO-induced cardiac hypertrophy, apoptosis and fibrosis. Primary cardiomyocytes of WT neonatal mice were pretreated with SB203580 (or with vehicle) prior to ISO stimulation, and results indicated that SB203580 pretreatment reduced the ISO-induced increase of cardiac hypertrophy markers, including atrial natriuretic peptide, brain natriuretic peptide and myosin heavy chain 7, cell cross sectional areas, and cardiomyocytes apoptosis (Figs. 7b–g and S9B–D). In addition, SB203580 pretreatment protected against ISO-induced cardiomyocyte mitochondrial structure

destruction (Fig. 7h) and ECM protein levels elevation in cultured cardiac fibroblasts (Figs. 7i and S9E) of WT neonatal mice. Furthermore, the data showed that SB203580 effectively inhibited MT disassembly (Figs. 7j, k and S9F) and mitochondrial translocation of p-MAP4 (Figs. 7l and S9G) of WT neonatal mouse cardiomyocytes after ISO stimulation.

We next evaluated the critical role of MAP4 phosphorylation in mediating the p38/MAPK regulation of cardiomyocyte apoptosis, MT dynamics and mitochondrial destruction (Fig. 7m–p). Primary cultured cardiomyocytes of WT neonatal mice were transiently transfected with MAP4(Ala), MKK6(Glu) or both, and the primary neonatal cardiomyocytes overexpressing MAP4(Ala) were more resistant than the CMV-null control to cardiomyocyte apoptosis (Fig. 7m and n), MT disassembly (Fig. 7o) and mitochondrial destruction (Fig. 7p) in response to MKK6(Glu) transfections. These findings proved the role of p38/MAPK as the upstream signaling of MAP4 phosphorylation and the critical role of MAP4 phosphorylation in the p38/MAPK activation mediated cardiac hypertrophy, apoptosis and fibrosis.

4. Discussion

The salient findings from our present study revealed that MAP4, the classical cytosolic MT-binding protein, increased phosphorylation in hypertrophied, compared with non-hypertrophied, ventricular tissue in the heart and drives pathological cardiac remodeling. This notion was proved in clinical patients, animal disease models, knockin mouse and cultured neonatal mouse cardiomyocytes or fibroblasts with a variety of research approaches. Our data suggested that MAP4 phosphorylation (S737 and S760) is universal increased following hypoxia and/or pressure overload, both of which are important stimulating factors for cardiac remodeling. The phosphorylation of MAP4 in mouse myocardium induces MT disassembly and mitochondrial translocation of p-MAP4, which leads to cardiac apoptosis shortly after birth, followed by discernible changes in mitochondrial swelling and dysfunction, myofilament disruption, and onset and progression of pathological cardiac remodeling with age.

Our earlier studies have indicated that MAP4 phosphorylation induced mitochondrial apoptosis in neonatal cardiomyocytes as responded to hypoxia *in vitro* [13]. In this study, we examined whether these changes corresponded to clinical patients and *in vivo* animal models. MAP4 phosphorylation and cardiac apoptosis were markedly increased in hypertrophic right ventricular tissues in hypoxemic patients with TOF compared with those in patients with normoxemia, suggesting a role of MAP4 phosphorylation in hypoxia-induced cardiomyocyte apoptosis in clinical patients. In order to elucidate the effect of right ventricular hypertrophy seen in TOF on MAP4 phosphorylation, we produced TAC mouse models to simulate pressure overload, and MI mouse models to recapitulate hypoxia. The data indicated that both hypoxia and pressure overload induced increased MAP4 phosphorylation (S737 and S760), accompanied with cardiac apoptosis. In addition, the p38/MAPK, which was demonstrated as the upstream regulator of MAP4 phosphorylation in our previous study and known as canonical signaling pathway involved in apoptosis [10,28,29], was not activated in MAP4 KI mice (Fig. S6). Thus, we inferred that the

Fig. 7. Role of p38/MAPK activation in MAP4 phosphorylation-induced cardiac hypertrophy, apoptosis and fibrosis. (a) Detection of p-M and p-P38 with or without SB203580 (SB) (5 μ M) in CMs. n = 5. (b) Protein markers of hypertrophy and p-P38 were detected using WB. n = 5. (c) Cross sectional areas of CMs were analyzed using cTnl and FITC-WGA co-staining. n = 5. (d and e) CMs apoptosis was detected by cTnl and fluorescein-TUNEL co-staining. Bar, 10 μ m. n = 5. (f) Protein levels of caspase-3 and t-caspase-3 were analyzed using WB. n = 5. (g) Detection of Cyt-c release from mitochondria. n = 5. (h) CMs mitochondria observed by TEM (black square indicated representative mitochondria). Bar, 1 μ m. (i) Markers of ECM were examined using WB. n = 5. (j) Poly/free tubulin was analyzed using WB. n = 5. (k) Representative confocal immunofluorescence images showing the MTs organization of the CMs. Bar, 10 μ m. The inserts showed high magnification images of the peripheral MT network. (l) Detection of p-M translocation to mitochondria with or without SB. n = 5. (m and n) CMs apoptosis was detected by cTnl and fluorescein-TUNEL co-staining after the cells were transiently transfected with MAP4(Ala), MKK6(Glu) or both. Bar, 10 μ m. n = 5. (o) Representative confocal immunofluorescence images showing the MTs organization of the CMs after the cells were transiently transfected with MAP4(Ala), MKK6(Glu) or both. Bar, 10 μ m. The inserts showed high magnification images of the peripheral MT network. (p) CMs mitochondria observed by TEM (black square indicated representative mitochondria) after the cells were transiently transfected with MAP4(Ala), MKK6(Glu) or both. Bar, 1 μ m. Data were shown as mean \pm SEM. The experiment was conducted 5 times. *P < 0.05, **P < 0.01, ***P < 0.001. P values were derived from one-way ANOVA with Bonferroni's post-test.

stimulation of hypoxia and/or pressure overload turns on p38/MAPK, leading to the phosphorylation of MAP4 and subsequently cardiac apoptosis.

Whether overt apoptosis was attributed to the MAP4 phosphorylation warrants further scrutiny. To test the effect of MAP4 phosphorylation *in vivo*, we generated a mouse model with mutated MAP4 by knocking in the coding sequence (S667A, S737E and S760E) in the 9th exon of MAP4 gene to simulate MAP4 with constantly phosphorylated S737 and S760, and unphosphorylated S667. At the age of 10–14 weeks, MAP4 KI mice displayed overt apoptosis, and cardiac hypertrophy occurred at the age of 30–34 weeks, along with thickened IVS and LV posterior wall, and increased markers for cardiac hypertrophy. Cardiac fibrosis characterized by increased ECM proteins and α -smooth muscle actin, emerged in MAP4 KI mice at 30–34 weeks and onwards. By 70–74 weeks of age, the pathological feature of cardiac hypertrophy worsened in MAP4 KI mice and accompanied with overt cardiomyocyte apoptosis, fibrosis and malfunction. The *in vitro* experiments indicated that MAP4(Ala) transfectants protected against cardiomyocyte apoptosis and fibroblast ECM production compared with cells transfected with CMV-null under ISO treatment in both WT and MAP4 KI group. The blood pressure exhibited no significant difference between two mouse genotypes both at the age of 30–34 and 70–74 weeks, which denoted that MAP4 phosphorylation triggered cardiac remodeling in the absence of hypertension.

In cardiac hypertrophy, a growing awareness has considered that abnormality of cardiac diastolic function is always recognized as an early character with or without systolic dysfunction [30]. With persistent stress, the heart changed from compensatory to decompensatory hypertrophy, with the gradually development of systolic dysfunction, and finally led to heart failure. There were no effective clinical measurements for the cardiac hypertrophy and diastole dysfunction [31], because the precise mechanisms how individual myocytes sensed the force pattern imposed by overload or hypoxia and subsequently transduced the signaling into sarcomere that resulted in cell thickening and lengthening were still elusive. Otherwise, most data suggested that cell death of cardiomyocytes may be the critical factor which transits the adaptive hypertrophy into maladaptive one [5,7]. However, exactly which signaling activated cardiomyocyte death and served as the critical factor between adaptive and maladaptive hypertrophy remained unclear. Our study may provide a new insight into the downstream effector of the overload or hypoxia stimuli, and the molecular mediator regulating the cardiomyocyte death in the pathophysiological process of cardiac remodeling.

The precise causality and mechanisms between MAP4 phosphorylation and cardiac remodeling deserve further elucidation. Cardiac hypertrophy could be provoked by mechanical, neurohumoral stimuli and genetic mutation. We examined GATA4 signaling, which plays an important role in cardiomyocyte survival, vasoactive peptide-induced hypertrophic changes and maintenance of cardiac function in the adult heart [32,33], and found that expression of GATA4 in MAP4 KI mice was comparable to WT littermates at different ages (Fig. S10). Accumulating data indicated the involvement of cytoskeleton in the pathogenesis of primary cardiomyopathy, including hypertrophic cardiomyopathy. Several mutated proteins of cytoskeletons such as α -cardiac actin, cTnI and β -myosin heavy chain are found linked to primary hypertrophic cardiomyopathy [34–36]. Clemen and colleagues reported that the mutated cytoskeleton caused abnormalities of myofilaments, ultimately resulting in cardiac hypertrophy [37]. In our hands, in addition to mitochondrial dysfunction, myofilament derangement could be seen in the MAP4 KI mice. Therefore, the MAP4 phosphorylation-induced MT disassembly may be involved in the myofilament derangement, and may participate in the onset and development of pathological cardiac remodeling.

In addition, our previous study depicted that mitochondrial translocation of p-MAP4 was the possible mechanism of apoptosis in cardiomyocytes [13], which was validated in the MAP4 KI mice in our

present study. Given that increased cardiomyocyte apoptosis occurred prior to cardiac remodeling in MAP4 KI mouse, consistent with the earlier notions [38], apoptosis may underlie MAP4 phosphorylation-induced cardiac remodeling. However, the relationship between phosphorylated MAP4-induced apoptosis and cardiac remodeling and its mechanism is far from clear. The role of calcium in the pathogenesis of hypertrophic cardiomyopathy has long been recognized, and the metabolism changes during hypertrophy is also a research hotspot. Considering the key role of mitochondria in calcium handling and cell metabolism, and the cardiomyocyte mitochondrial dysfunction and apoptosis appeared ahead of cardiac hypertrophy in MAP4 KI mice, maybe we could work on that from mitochondria and its related calcium handling and cell metabolism in future.

It should be noted that in our current study, the pathological and echocardiographic observations showed hard evidences of LV remodeling, and the heart tissue samples applied in this study were mainly from the LV free wall. While TOF patients, which were characterized by right ventricular hypertrophy, also showed increased MAP4 phosphorylation and cardiac apoptosis, indicating a possible correlation between MAP4 phosphorylation and right ventricular hypertrophy. However, we could not provide *in vivo* echocardiographic data of right ventricular because of the technology limitation for the time being, and we are trying to improve the echocardiographic measurement and may show these data in future. In addition, we used neonatal rather than adult cardiomyocytes in this study considering that the living time of adult cardiomyocyte was limited and cannot be applied for MAP4(Ala) adenovirus transfection. However, it must be realized that adult cardiomyocyte was more appropriate for investigating age-related cardiac remodeling, stretch-induced hypertrophy and electrophysiological experiment. How to search for a win-win solution needs further thinking and solving. The other defect of our current study is that the MAP4 KI mouse model is systemic KI model. Although no significant differences on the biochemistry parameters between the two genotypes of mice were noted with aging (till to 74 weeks), we cannot exclude the potential influences of the other tissues and organs on cardiac remodeling. The time- and tissue-specific MAP4 phosphorylation mice may help us to solve the problem in future.

In summary, findings reported in our study reveal that MAP4 phosphorylation may serve as a springboard for the pathogenesis of multiple cardiomyopathies including cardiac hypertrophy, fibrosis, diastolic and systolic dysfunction, suggesting its therapeutic potentials in these comorbidities. Further study is warranted to further clarify the precise mechanisms for the development of therapeutic interventions targeting MAP4 phosphorylation to ameliorate maladaptive cardiac remodeling and development of heart diseases.

Funding sources

This work was supported by the Key Program of National Natural Science Foundation of China (No.81430042) and National Natural Science Foundation of China (No.81671913).

Declaration of interests

None exist.

Author contributions

Y.H. supervised the work; L.L. and J.H. designed the experiments with help from J.R., J.Z., D.Z. and X.J.; L.L., J.H. performed the experiments with help from Q.Z., X.Z., J.Z. and J.J.; X.W. collected the TOF heart tissues; L.L., B.C., H.M. and J.H. analyzed the data; L.L., J.H. and J.R. co-wrote the manuscript. All authors discussed the results and commented on the manuscript.

Appendix A. Supplementary data

Supplementary data to this article can be found online at <https://doi.org/10.1016/j.ebiom.2018.10.017>.

References

- [1] Braunwald E. The war against heart failure: the Lancet lecture. *Lancet* 2015;385:812–24.
- [2] McKinsey TA, Olson EN. Toward transcriptional therapies for the failing heart: chemical screens to modulate genes. *J Clin Invest* 2005;115:538–46.
- [3] Fielitz J, Kim MS, Shelton JM, et al. Requirement of protein kinase D1 for pathological cardiac remodeling. *Proc Natl Acad Sci U S A* 2008;105:3059–63.
- [4] Oka T, Akazawa H, Naito AT, Komuro I. Angiogenesis and cardiac hypertrophy: maintenance of cardiac function and causative roles in heart failure. *Circ Res* 2014;114:565–71.
- [5] Kimura TE, Jin J, Zi M, et al. Targeted deletion of the extracellular signal-regulated protein kinase 5 attenuates hypertrophic response and promotes pressure overload-induced apoptosis in the heart. *Circ Res* 2010;106:961–70.
- [6] Saito T, Asai K, Sato S, et al. Autophagic vacuoles in cardiomyocytes of dilated cardiomyopathy with initially decompensated heart failure predict improved prognosis. *Autophagy* 2016;12:579–87.
- [7] Gercek M, Gercek M, Kant S, et al. Cardiomyocyte hypertrophy in arrhythmogenic cardiomyopathy. *Am J Pathol* 2017;187:752–66.
- [8] Li Y, Ge S, Peng Y, Chen X. Inflammation and cardiac dysfunction during sepsis, muscular dystrophy, and myocarditis. *Burns Trauma* 2013;1:109–21.
- [9] Li L, Hu J, He T, et al. p38/MAPK contributes to endothelial barrier dysfunction via MAP4 phosphorylation-dependent microtubule disassembly in inflammation-induced acute lung injury. *Sci Rep* 2015;5:8895.
- [10] Hu JY, Chu ZG, Han J, et al. The p38/MAPK pathway regulates microtubule polymerization through phosphorylation of MAP4 and Op18 in hypoxic cells. *Cell Mol Life Sci* 2010;67:321–33.
- [11] Drewes G, Ebneth A, Mandelkow EM. MAPs, MARKs and microtubule dynamics. *Trends Biochem Sci* 1998;23:307–11.
- [12] Illenberger S, Drewes G, Trinczek B, et al. Phosphorylation of microtubule-associated proteins MAP2 and MAP4 by the protein kinase p110mark. Phosphorylation sites and regulation of microtubule dynamics. *J Biol Chem* 1996;271:10834–43.
- [13] Hu J, Chu Z, Han J, et al. Phosphorylation-dependent mitochondrial translocation of MAP4 is an early step in hypoxia-induced apoptosis in cardiomyocytes. *Cell Death Dis* 2014;5:e1424.
- [14] Ebneth A, Drewes G, Mandelkow EM, Mandelkow E. Phosphorylation of MAP2c and MAP4 by MARK kinases leads to the destabilization of microtubules in cells. *Cell Motil Cytoskeleton* 1999;44:209–24.
- [15] Srsen V, Kitazawa H, Sugita M, et al. Serum-dependent phosphorylation of human MAP4 at Ser696 in cultured mammalian cells. *Cell Struct Funct* 1999;24:321–7.
- [16] Kitazawa H, Iida J, Uchida A, et al. Ser787 in the proline-rich region of human MAP4 is a critical phosphorylation site that reduces its activity to promote tubulin polymerization. *Cell Struct Funct* 2000;25:33–9.
- [17] Raingeaud J, Whitmarsh AJ, Barrett T, Derijard B, Davis RJ. MKK3- and MKK6-regulated gene expression is mediated by the p38 mitogen-activated protein kinase signal transduction pathway. *Mol Cell Biol* 1996;16:1247–55.
- [18] Huang ZP, Kataoka M, Chen J, et al. Cardiomyocyte-enriched protein CIP protects against pathophysiological stresses and regulates cardiac homeostasis. *J Clin Invest* 2015;125:4122–34.
- [19] Wang WE, Yang D, Li L, et al. Prolyl hydroxylase domain protein 2 silencing enhances the survival and paracrine function of transplanted adipose-derived stem cells in infarcted myocardium. *Circ Res* 2013;113:288–300.
- [20] Chowdhury A, Hasselbach L, Echtermeyer F, Jyotsana N, Theilmeier G, Herzog C. Fibulin-6 regulates pro-fibrotic TGF-beta responses in neonatal mouse ventricular cardiac fibroblasts. *Sci Rep* 2017;7:42725.
- [21] Tsutsui H, Tagawa H, Kent RL, et al. Role of microtubules in contractile dysfunction of hypertrophied cardiocytes. *Circulation* 1994;90:533–55.
- [22] Brandt T, Mourier A, Tain LS, Partridge L, Larsson NG, Kuhlbrandt W. Changes of mitochondrial ultrastructure and function during ageing in mice and *Drosophila*. *Elife* 2017;6:e24662.
- [23] Matsuda T, Zhai P, Maejima Y, et al. Distinct roles of GSK-3alpha and GSK-3beta phosphorylation in the heart under pressure overload. *Proc Natl Acad Sci U S A* 2008;105:20900–5.
- [24] Zhu L, Wang Q, Zhang L, et al. Hypoxia induces PGC-1alpha expression and mitochondrial biogenesis in the myocardium of TOF patients. *Cell Res* 2010;20:676–87.
- [25] Ghorbel MT, Cherif M, Jenkins E, et al. Transcriptomic analysis of patients with tetralogy of Fallot reveals the effect of chronic hypoxia on myocardial gene expression. *J Thorac Cardiovasc Surg* 2010;140:337–45 [e26].
- [26] Creemers EE, Pinto YM. Molecular mechanisms that control interstitial fibrosis in the pressure-overloaded heart. *Cardiovasc Res* 2011;89:265–72.
- [27] Thum T, Gross C, Fiedler J, et al. MicroRNA-21 contributes to myocardial disease by stimulating MAP kinase signalling in fibroblasts. *Nature* 2008;456:980–4.
- [28] See F, Thomas W, Way K, et al. p38 mitogen-activated protein kinase inhibition improves cardiac function and attenuates left ventricular remodeling following myocardial infarction in the rat. *J Am Coll Cardiol* 2004;44:1679–89.
- [29] Zhang S, Ren J, Zhang CE, Treskov I, Wang Y, Muslin AJ. Role of 14-3-3-mediated p38 mitogen-activated protein kinase inhibition in cardiac myocyte survival. *Circ Res* 2003;93:1026–8.
- [30] Fraysse B, Weinberger F, Bardswell SC, et al. Increased myofilament Ca²⁺ sensitivity and diastolic dysfunction as early consequences of Mybpc3 mutation in heterozygous knock-in mice. *J Mol Cell Cardiol* 2012;52:1299–307.
- [31] McNally EM, Golbus JR, Puckelwartz MJ. Genetic mutations and mechanisms in dilated cardiomyopathy. *J Clin Invest* 2013;123:19–26.
- [32] Liu Y, Wang Z, Xiao W. MicroRNA-26a protects against cardiac hypertrophy via inhibiting GATA4 in rat model and cultured cardiomyocytes. *Mol Med Rep* 2016;14:2860–6.
- [33] Perrino C, Rockman HA. GATA4 and the two sides of gene expression reprogramming. *Circ Res* 2006;98:715–6.
- [34] Witjas-Paalberends ER, Piroddi N, Stam K, et al. Mutations in MYH7 reduce the force generating capacity of sarcomeres in human familial hypertrophic cardiomyopathy. *Cardiovasc Res* 2013;99:432–41.
- [35] Muller M, Mazur AJ, Behrmann E, et al. Functional characterization of the human alpha-cardiac actin mutations Y166C and M305L involved in hypertrophic cardiomyopathy. *Cell Mol Life Sci* 2012;69:3457–79.
- [36] Ford SJ, Mamidi R, Jimenez J, Tardiff JC, Chandra M. Effects of R92 mutations in mouse cardiac troponin T are influenced by changes in myosin heavy chain isoform. *J Mol Cell Cardiol* 2012;53:542–51.
- [37] Clemen CS, Stockigt F, Strucksberg KH, et al. The toxic effect of R350P mutant desmin in striated muscle of man and mouse. *Acta Neuropathol* 2015;129:297–315.
- [38] Teiger E, Than VD, Richard L, et al. Apoptosis in pressure overload-induced heart hypertrophy in the rat. *J Clin Invest* 1996;97:2891–7.